Effect of Coal Particle Size on the Temperature and Pressure of Low Temperature Carbonization Square Furnace: A Combined Computational and Industrial Practice Study

Yu-fei Wang
Yulin University
Qian-qian Liu
Yulin University
Long Yan (ylyanlong@126.com)
Yulin University
Yong Dan
Northwest University
Wen-xing Mi
Northwest University
Jian Li
Yulin University
Yong Gao
Yulin University
Feng Fu
Yan'an University
Qiu-li Zhang
Xi'an University of Architecture and Technology
Jun-li Liu
Shenmu Sanjiang Coal Chemical Indusitry Co., Ltd
Wen-zhi Shang
Shenmu Sanjiang Coal Chemical Industry Co., Ltd

Research

Keywords: Carbonization square furnace, Particle size, Temperature field, Pressure field, Numerical simulation

Posted Date: November 9th, 2020

DOI: https://doi.org/10.21203/rs.3.rs-102587/v1

Abstract

Three-dimensional computational fluid dynamics according to the actual size of carbonization square furnace was performed, the standard k-ε model, the finite-rate/eddy-dissipation model and the P1 radiation model were adopted to simulate the flow of gases, the combustion of gas mixture and the heat transfer process, a mathematical model for square furnace was established when the porous medium model was selected for approximate replacement of coal seams in the furnace. The temperature and pressure fields with eight particle sizes of coal were also investigated and compared to five groups of conditions in the actual industrial production. The results showed that furnace witnessed dropped temperature, increased pressure, and gradually accelerated decline in the volume percentage of the carbonization zone with decreasing particle size of coal. However, the trends of flow field distribution were similar under different particle sizes, the maximum temperature and pressure presented an approximately linear decline and an approximately exponential growth, respectively. The temperature difference at the same height gradually narrowed with the gradual increase in the coal seam height under the same particle size. Moreover, the comparison between the numerical simulation results and industrial practice revealed a temperature and pressure error both lower than 6.25% and 12.8%, respectively.

1. Introduction

Carbonization furnaces are major devices used in the low temperature carbonization production and can be classified into external heating type, internal heating type, and hybrid heating type according to heating modes [1]. The vertical internally heated low temperature carbonization square furnace (SJ carbonization furnace) developed by Shenmu Sanjiang Coal Chemical Industry Co., Ltd. is designed on the basis of Woodall-Duckham Gasifier after focusing on the advantages of relevant furnace models and the experience from local production practice worldwide. It is a new “native” furnace model that can adapt to the characteristics of low metamorphic coal in northern Shaanxi Province [2]. In general, pyrolysis reactors for the heat transfer and mass transfer require raw coal with different particle sizes [3]. SJ carbonization furnace can obtain a relatively high proportion of target product in the pyrolysis of lump coal with the particle size in the range 30~80 mm [2, 4]. However, when it comes to the large amount of raw coal smaller than 30 mm in size left after fully mechanized mining, SJ carbonization furnace fails to provide efficient pyrolysis and may even result in blocking [2, 5, 6]. This suggests that although temperature and pressure are the key parameters for SJ low temperature carbonization furnace and main factors affecting the yield and quality of coal tar, semi-cock, and other chemical products, the primary cause of pressure variations in a furnace in the actual factory production is the particle size of the as-fired coal . In addition, the development of SJ low temperature carbonization technology is mainly derived from practice and there is an absence of laboratory tests and sound theoretical support [2, 4, 7]. Therefore, directly testing the key parameters (temperature and pressure) in low temperature carbonization process is very difficult. In particular, there is a lack of guidance over the simulation of temperature and pressure field distribution after feeding with regard to coal with a small particle size (smaller than 30 mm).

Computational fluid dynamics (CFD), as a powerful numerical simulation study method in the international community, has been widely applied to study the temperature and pressure fields of some combustion and industrial furnaces [8-10]. For instance, Guo et al. numerically simulated the coking process of regenerative coke ovens and obtained the time-dependent temperature distribution in coking chamber [11]. Slezak et al. performed a numerical simulation of the two-stage gasification process with the FLUENT software, and the relationship between the particle size, the density of pulverized coal and the flow field, the components of the outlet, the residence time of pulverized coal in the furnace is obtained [12]. Liu et al. simulated the temperature field distribution in the impinging-type low temperature combustion chamber of a self-developed low temperature carbonization furnace for low-rank coal and optimized its structure [13]. However, the numerical simulation of the flow fields of SJ low temperature carbonization furnaces is rarely reported, and only Zhang et al. from Xi'an University of Architecture and Technology (XAUAT) simulated the effect of different air/gas ratios on the temperature fields of low temperature carbonization furnaces [14].

In this study, the physical model and meshing based on productive furnaces were established, and a suitable mathematical model was selected to simulate the temperature and pressure fielddistribution in the SJ furnace after feeding coal with different particle sizes. By comparing the CFD simulation values and factory test data, the reason of blocking in the furnace was rationalized, the cost of blind testing was saved, and a theoretical foundation for improving the furnace model and obtaining the ideal target product was put forth.

2. Establishment Of Models And Determination Of Boundary Conditions Andalgorithms

2.1 Establishment of physical models

Figure 1 shows the structure of SJ internal heating low temperature carbonization furnace. A large-cavity design is adopted, and the top to bottom consists of drying segment, carbonizing segment, and cooling segment. The as-fired coal first enters from the coal hopper and then passes through the cavity after gradual drop during service. There are four of intact grid walls and two of semi-grid walls below the cavity. The as-fired coal gas and air are mixed in a certain ratio, and the mixture is uniformly fed into the furnace from both sides of the grid walls. A portion of the carbonization gas flows back and is used as the as-fired coal gas. It quickly combusts in the furnace and generates high temperature heat-carrier gases with the assistance of insufficient oxygen, and then coal seams are heated one by one. The coal after the carbonization passes through the coke pusher, lands in the coke quenching pond via the coke inlet, and is dried to obtain the finished semi-coke product.

The ICEM (Integrated Computer Engineering and Manufacturing code) of the ANSYS Fluent software was used in this study to perform three-dimensional (3D) modeling and meshing according to the effective size of SJ furnace with dimensions of 5.50 m × 2.80 m × 6.50 m (length × width × height), and the effective volume of SJ furnace was about 100 m^3. In fact, the actual size of SJ furnace was

7.42 m × 4.52 m × 7.00 m (length × width × height), this means that the SJ furnace is complicated in structure and large in size, the gas collecting mantle, coal-gas water seal tank, ascending bridge pipe, auxiliary coal box, and other devices in the furnace were configured, all of which participated in the heat transfer and disturbed pressure distribution to some extent. It would be extremely difficult to precisely simulate the flow field of the whole SJ furnace in this case. The whole furnace cavity was selected as the computational domain, and the effect of devices in the furnace cavity was neglected in this study, mostly because the combustion reaction in the furnace occurred at the bottom of the furnace cavity and other devices did not experience any chemical reaction and exerted only an insignificant effect on the flow field distribution in the furnace. The 3D model and the meshing for SJ furnace is shown in Figure 2, separately, where the three directions of x, y and z represent the length, width and height of the furnace, respectively.

2.2 Selection of mathematical models

The combustion of coal gas in a carbonization furnace is a complicated multi-phase turbulent combustion process that involves many physical and chemical reactions [2]. The fluid flow in the furnace is a typical 3D multi-component gas–solid two-phase turbulent flow. The combustion here refers to the combustion of multi-component gas phase, and combustion reaction and turbulent flow correlate and interact with each other. When CFD is used to numerically simulate the processes in a furnace, establishing a reliable mathematical model is especially important.

The flow of gas in the SJ carbonization furnace can be regarded as turbulent motion and simulated by the standard k-ε model [14-16]. The combustion of the as-fired gas mixture in a carbonization furnace can be simulated with the finite-rate/eddy-dissipation model [17, 18], which is a component transfer model. The combustion temperature of coal gas in the SJ furnace is relatively high in actual production, and the amount of radiative heat transfer at high temperature is directly proportional to the biquadrate of temperature. The heat transfer between the coal seams and high temperature gases is dominated by radiative heat transfer and simulated with the P-1 radiation model [19, 20]. The coal seams in the SJ carbonization furnace cavity can be approximated to porous mass and simulated with the porous medium model [21, 22].

2.3 Determination of boundary conditions and algorithms

(1) Inlet boundary conditions

Given the flow at flow field inlet, both the mass inlet and velocity inlet boundary conditions can be used according to the method of setting inlet boundary conditions provided by the ANSYS Fluent software; however, velocity inlet conditions can not apply to incompressible flow. Thus, its boundary condition type is set as the mass flow inlet conditions in this study [23]. The nozzle section of the gas mixture of coal gas and air on both sides of a grid wall as inlet were adopted according to the equivalent area method.

(2) Outlet boundary conditions

The boundary conditions applicable to the outlet of the SJ low temperature carbonization furnace include pressure outlet conditions and free flow conditions according to the method of setting outlet boundary conditions provided by the ANSYS Fluent software[24]. Measuring the flue gas pressure at the outlet before solving the practical engineering is difficult; therefore, the outflow boundary conditions can be assumed to obey fully developed flow and the diffusive fluxes of all the flow variables (except pressure) have a gradient of zero along the flow direction. Following this idea, the outlet boundary conditions were set as the outlet flow in this study.

(3) Wall boundary conditions

The method by the ANSYS Fluent software usually divides the near-wall area in viscous fluid computation into three layers, including the viscous sublayer near wall surface, the fully turbulent layer in the outer zone, and the hybrid layer in the middle [25]. The flow in the near-wall area is approximate to laminar flow, and the effect of the wall surface on the flow is relatively small in the SJ carbonization furnace [26]. The standard wall function method was adopted to simulate the flow in the near-wall area, and the conditions without velocity slip and mass osmosis were introduced for fixed wall surface, and the wall thickness and wall surface temperature variations in the process of heat transfer were neglected, and the actual temperature was set as 300 K according to the working conditions.

According to the flows, the mixing ratio and volume fractions of the as-fired coal gas and air, the mass fractions of various gases, and their total flow were computed. The components of the as-fired coal gas are listed in Table 1.

Table 1 Volumetric composition of as-fired coal gas (%).

H_2	CO	CO_2	CH_4	C_2H_6	C_2H_4	N_2
28.3	16.0	10.0	7.3	0.2	0.3	37.9

The porosity, inertial resistance, viscous resistance, and other parameters of the coal seams were deduced based on the particle size of as-fired coal, and the SIMPLE algorithm, a pressure-velocity coupling algorithm, was adopted as its computation method [27]. The ratio of the as-fired coal gas/air was kept constant in the light of actual production conditions, and the particle size of the as-fired coal (represented by D) was changed and set as 40, 35, 30, 25, 20, 15, 10, and 5 mm to simulate the temperature and pressure fields in the furnace. In addition, a comparative analysis with the test results of five groups of coal with different particle sizes provided by Shenmu Sanjiang Coal Chemical Industry Co., Ltd was conducted. The particle size range distribution and average particle size of the coal selected by Shenmu Sanjiang Coal Chemical Industry Co., Ltd. are listed in Table 2.

Table 2 Particle size ranges of differentas-fired coal and their average particle size.

D/mm	10-60	10-30	5-30	3-30	0-30
/mm	32.44	16.97	14.76	12.55	8.13

To fully reflect the temperature and pressure field distribution in the furnace, the sections y = 1.4 m and x = 2.75 m were selected as examples to investigate the flow field variations in the furnace because there were the center sections of the as-fired gas inlets in y-direction and x-direction, respectively.

3. Results And Discussion

3.1 Effect of different particle sizes of coal on the temperaturefield distribution of furnace's longitudinal and transverse center sections

When the as-fired coal particle size was set at 40, 35, 30, 25, 20, 15, 10, and 5 mm, the temperature field distribution of y-direction and x-direction center sections are shown in Figure 3 and 4, which is for the numerical simulation results of the SJ carbonization furnace. The temperature field distribution in the furnace cavity was symmetric, chiefly from Figure 3 and 4, because the structure of the SJ furnace was symmetric and materials basically entered various feeding inlets in a uniform manner. When the coal with the same particle size entered the SJ furnace, the furnace cavity as a whole presented an increasing trend first and decreasing afterwards from the peripheral zone of the inlet to the furnace top. However, the temperature at the inlet of the gas mixture of the coal gas and air was relatively low, and the maximum temperature in the furnace emerged at the joints between the grid walls and furnace cavity (red in the zone) while the minimum temperature occurred near the wall surface. The reason was that the study sections y = 1.4 m and x = 2.75 m selected in Figure 3 and 4, respectively, were the center sections of the as-fired gas inlets, and the gas mixture of the coal gas and air fed into the grid walls after mixing via a branch mixer had a relatively low temperature, resulting in the relatively low temperature at the gas mixture inlet. The gas mixture gradually increased in the process of upward motion to the kindling points of various components of coal gas with its spreading, and carbon monoxide, hydrogen, methane, ethylene, acetylene, and other gases engaged in the combustion reaction with oxygen in the air at the joints between the grid walls and furnace cavity, releasing a large amount of heat and gradually elevated the furnace temperature (to the maximum temperature upon complete combustion). After that, these high temperature gases were used as heat-carriers, which engaged in heat transfer with coal seams from bottom up, gradually declining the temperature in the furnace cavity. The wall surface was far away from high temperature heat sources and ceaselessly emitted heat to the outside area; therefore, it had the minimum temperature [28]. When different particle sizes of coal entered the SJ furnace, the bulk temperature in the furnace cavity decreased with decreasing particle size, but the overall temperature distribution trends were similar. This was probably because the decrease in the as-fired coal particle size increased the bulk density of coal seams in the furnace, narrowed the gas channels, intensified resistance, and lowered the heat transfer efficiency, and thus decreased the temperature [2, 3, 29, 30].

D = 20 mm was taken as an example to analyze the flow field distribution in the high temperature zones. The partial enlarged drawings of x-direction high-temperature zone section x = 2.75 m, y-directionhigh-temperature zone section y = 1.4 m and z-direction high temperature zone section z = 0 m (D = 20 mm) are shown in Figure 5. The high-temperature zone took the combustion of coal in two opposite feed inlets as a combustion point and regarded the boundary of the two semi-grid walls as a combustion unit for the convenience of study. As shown in Figure 5(a), the high temperature zone of the central combustion unit was approximately “tripod-shaped”, that is the temperatures of the combustion points on the two sides were basically equal (about 50 K) and lower than the temperature of the combustion point in the center. This was probably because the center released less heat and had slightly more combustion gas within a combustion unit [31]. Figure 5(b) shows that the maximum temperatures of the five combustion units were close to each other; however, the area of high-temperature zone continuously expanded from the furnace center to its two sides and diffused combustion zones emerged. This was probably because the high-temperature point at the center of the furnace cavity directly faced the gas outlet of the furnace, and the furnace pressure ascended progressively at small amplitude from the center to the two sides, gradually decreasing the gas flow rate from the center to both the sides [32]. The return coal gas with the assistance of oxygen combusted at a higher rate at the furnace center and was completely combusted in a relatively small zone at an earlier point.As shown in Figure 5(c), the maximum temperature of each combustion point emerged at the symmetric center of the two semi-grid walls, the maximum temperatures of the five combustion units all occurred at the y-direction of the SJ furnace, and the wall surface and combustion unit interface exhibited the minimum temperatures. This was because the feed inlets were in paired layout, the gas mixture began to move upwards, such intense mixing increased the turbulence intensity of updraft and facilitated the combustion when it entered the furnace from two opposite channels and experienced intense mixing at the center of the combustion unit [33]. On section z = 0, it reached its kindling point and received complete combustion. The combustion unit interface and wall surface were far away from the combustion points; therefore, their temperatures were relatively low.

3.2 Temperature distribution characteristics of longitudinal center section at different coal seam heights

Coal seams with the heights z = 0, 0.5, 1, 2, and 4 m were taken as the study objects. The temperature distribution at each height is shown in Figure 6. When the boundary between two of semi-grid walls was taken as the study object, the temperature distribution of the longitudinal center section at different coal seam heights could be roughly divided into three stages with increasing coal seam height. Stage I: At the height z = 0 m, coal seam temperatures presented a symmetric distribution on the whole, and the coal seam temperatures of the five combustion units all showed an “inverted v-shaped” distribution. The maximum temperatures were approximately equal (≈1,030 K) and located at the symmetric center of two semi-grid walls. The temperatures at the symmetric centers of the grid walls and the wall surface on both sides were relatively low, and the temperature difference between the coal seams at the same height reached the maximum level in this case. Stage II: The wave peaks at the coal seam heights of z = 0.5 and 1 m gradually became gentle with increasing coal seam height, and the high temperature point positions moved towards the furnace center step by step. In addition, high temperature points were reduced into

four high temperature wave peaks in a symmetric distribution, and the maximum temperature was close to the symmetric centers of the grid walls on the both sides of the furnace. When z = 1 m, the maximum temperature difference between the high temperaturepoints was approximately 100 K. Stage III: When the coal seam height exceeded z = 2 m, the temperature at the furnace center (except the two sides of furnace close to wall surface) was relatively uniform and gradually declined with rising coal seam. This was because the gas mixture of the coal gas and air began to combust at the height z of approximately 0 m when it was fed into the furnace. During the rise of the extremely hot heat-carriers, the gas at the center was moving at a faster pace than that on both sides. As a result, coal seams presented a symmetric temperature distribution, and the temperature at the center was higher than that on each side in stage I. To be specific, the temperatures at the symmetric centers of grid walls were low, primarily because they were far away from the heat sources and the unsmooth cusp-shaped grid walls blocked the transverse flow of gas [14]. In stage II, the temperature difference between the coal seams presented a gradually narrowing trend in the process of coal seam height gradually increasing to 0.5 m and 1 m. This was because the heat transfer between the coal seams and gas was dominated by radiative heat transfer in the high-temperature zone of the furnace, and higher temperature led to quickerheat transfer, resulting in a relatively significant temperature difference [34]. The reduction in the high temperature points into four high temperature wave peaks in symmetric distribution resulted from the rising high temperature gases converging on four intact grid walls, and the maximum temperatures were close to the symmetric centers of the grid walls on both sides due to the emergence of diffused combustion zones on the two sides. The height z = 1 m was at the centers of the diffused combustion points, creating a temperature difference between the high temperature points to be the maximum. In stage III, the temperature difference at the furnace center was relatively uniform principally because higher coal seams decreased the temperature in the SJ furnace. The heat transfer between relatively low thermal conductivity of coal and gas was dominated by heat transmission, and the rate of heat transfer was relatively balanced [14]. It is also clear that the smaller the distance between the coal seam height and wall surface, the lower the temperature. The wall surface constantly emitted heat, resulting in a relatively low temperature.

3.3 Relationship between the maximum temperature in furnace and particle size

According to the temperature field simulation results of different particle sizes of the as-fired coal, the temperature in the furnace cavity decreased with decreasing particle size. The correspondence between the maximum temperature in the furnace and as-fired coal particle size is shown in Table 3, indicating that the maximum temperature Tmax gradually decreased with decreasing as-fired coal particle size. When particle size was 40 mm, the maximum temperature was 1,148 K; when particle size was 5 mm, the maximum temperature decreased to 921 K.

Table 3 Maximum temperatures of different particle sizes of as-fired coal.

D/mm	40	35	30	25	20	15	10	5
T_{max}/K	1148	1115	1092	1063	1006	976	950	921

The relationship between the maximum temperature in the furnace and particle size is shown in Figure 7. Clearly, the maximum temperature in the furnace decreased linearly with decreasing coal particle size, mainly due to the variations in the porosity of coal seams. When the as-fired coal particle size decreased from 40 m to 5 mmthe true density and bulk density of different particle sizes of coal were experimentally measured and substituted into the computational Eq. (1) to calculate the porosity of coal of different particle sizes [35, 36], and the results are listed in Table 4:

$$P=\frac{\rho_0-\rho}{\rho_0}\times 100\% \quad (1)$$

where P is the porosity of the coal, ρ_0 is the true density of the coal, and ρ is the bulk density of the coal.

As listed in Table 4, the porosity of coal seams in the furnace gradually decreased from 0.395 to 0.263 with decreasing coal particle size, increasing the resistance coefficient of coal seams, which further increased the resistance to the passage of gas, reduced the flow rate of rising gases, quickly combusted the coal and ultimately lowered the maximum temperature[37].

Table 4 True density, bulk density, and porosity of different particle sizes of coal.

D/mm	40	35	30	25	20	15	10	5
/(kg/m^3)	1227	1227	1227	1227	1227	1227	1227	1227
(kg/m^3)	742	763.2	785.3	802.5	822.1	838	862.6	904.3
P	0.395	0.378	0.36	0.346	0.33	0.317	0.297	0.263

After linearly fitting the relationship between the maximum temperature in the furnace and as-fired coal particle size, the fitting curve showed a relatively high correlation coefficient, i.e., 0.9937. The fitting equation is as follows:

$$T_{max} = 6.1238D + 906.7143 \quad (2)$$

3.4 Relationship between the temperature range percentage in the furnace and particle size

The medium and low temperature carbonization of coal refers to the thermal decomposition of coal into coal gas, coal tar and semi-coke in an air-free environment after being heated in the range 773~1,023 K [1, 38, 39]. The pyrolysis process of coal has been extensively investigated, and carbonization is divided into three stages according to temperature, including normal temperature to 573 K, 573~773 K, and 773~1,023 K. The stage of normal temperature to 573 K mainly provides drying and desorption to remove free water and adsorbed gases. The second stage mainly generates and discharges a large amount of volatiles through decomposition and depolymerization. To be specific, the precipitates amount of coal tar

can reach the largest when the temperature is about 723 K [3, 39, 40]. In the range 773~1,023 K, mainly plastic mass experiences polycondensation and curing reactions and generates semi-coke [3, 39, 40]. Figure 8 shows the volume percentage distribution in various temperature ranges when the as-fired coal particle size varied in the range 40~ 5 mm.

When D = 40 mm, the volume percentages of temperature ranges a, b, c and d in the temperature field were 45.21%, 34.01%, 18.68% and 2.1%, respectively. As shown in Figure 11, when the as-fired coal particle size decreased from 40 mm to 5 mm, the percentage of temperature range gradually increased from 45.21% to 62.23% at an increasingly faster pace. Specifically, in the sub-range 10~5 mm, the increasing rate was the highest (~6%) and the area percentage of temperature range exceeded 60%. In the range 40~10 mm, the volume percentage of temperature range b in the temperature field approximately decreased linearly at a rate of 1%, and the volume percentage of temperature range b dropped by approximately 2% when particle size decreased from 10 mm to 5 mm, in which case it reached 25.92%. Temperature range c served as an important reference index of the normal efficient running of SJ low temperature carbonization furnace and is further analyzed as follows. The volume percentage of temperature range d was relatively low and continuously narrowed. It dropped to zero when particle size fell below 20 mm, because the induced variations in the volume percentages of various temperature ranges was the same that gave rise to the relationship between the maximum temperature in the furnace and particle size [41].

Figure 9 shows the variation trend of the volume percentages of the carbonization zone (773~1,023 K) for different particle sizes of the as-fired coal, indicating that the variation trend in the volume percentage of the carbonization zone could be divided into three stages when the as-fired coal particle size decreased from 40 mm to 5 mm. Stage I (40~20 mm): In this stage, the volume percentage of the carbonization zone decreased, but only by a very small amplitude, mainly because the varied particle size was still relatively large and the pressure difference in furnace changed slightly. As a result, the effect on the flow of gas in the furnace was not obvious and combustion was basically unaffected; therefore, the carbonization zone did not experience any obvious variation in the area. In addition, a high-temperature zone higher than 1,023 K emerged at this point, and radiation also exerted a vital effect on the carbonization zone. Stage II (20~10 mm): In this stage, the area percentage of the carbonization zone basically decreased linearly at a rate of approximately 3%, because the pressure difference in the furnace cavity relatively increased and gas flow rate declined to some extent with decreasing particle size, accompanied by weakened combustion reaction, constantly lowered the maximum temperature, and gradually diminished the radiation capacity [41]. Stage III (10~5 mm): This stage saw a significant decrease in the volume percentage of the carbonization zone approximately in the range 4~11.85%. For the small particle size, the porosity of coal seams declined substantially, while the gas flow resistance increased significantly, thus the combustion was incomplete, and blocking might have taken place at 5 mm [41].

3.5 Effect of different particle sizes of coal on the pressure field distribution of furnace's longitudinal center section

Figure 10 shows the pressure field distribution of y-direction center section for the numerical simulation results of the SJ carbonization furnace when the as-fired coal particle size was set at 40, 35, 30, 25, 20, 15, 10, and 5 mm. As shown in Figure 10, the pressure in the furnace increased with decreasing particle size when different particle sizes coal entered the furnace, but the distribution trends were similar. At the same coal seam height, pressures were basically equal, because the porosity of porous medium declined with decreasing particle size, and the permeation property of gases weakened [41]. Considering the similar trends of pressure distribution in the furnace, D = 20 mm was taken as a typical case to analyze the distribution law of the pressure in the SJ furnace along the coal seam height direction.

Figure 11 shows the relationship between the coal seam heights and the pressure in the furnace when D = 20 mm. It is evident that the pressure in the furnace presented an overall declining trend with increasing coal seam height when the same particle size of coal entered the furnace; however, the pressure showed a small-amplitude increase with increasing height in the vicinity of the coal seam height h = 1.05 m, largely because the coal seam height of 1.05 m was the gas inlet of SJ carbonization furnace, resulting in a relatively high temperature around the inlet. When the coal seam height h reached 5.5 m, the pressure in the SJ furnace dropped quickly, because the coal seam served as the gas outlet on the furnace top after its height h exceeded 5 m, and gas resistance was particularly low. Besides, a negative-pressure device (whose pressure was slightly lower than atmospheric pressure) was used to collect gases at the furnace outlet, resulting in a quick pressure drop and causing the minimum pressure to drop below atmospheric pressure. The pressure in the furnace cavity (except at the outlet of the furnace top) presented an approximately linear decline, primarily because the gas flow rate u across the porous medium zone remained approximately constant, and the pressure drop $\triangle P$ was directly proportional to the gas flow rate u according to the porous medium model [21, 42].

The pressure in the furnace cavity increased with decreasing particle size according to the pressure field simulation results of different particle sizes of the as-fired coal. Table 5 lists the correspondence between the maximum pressure in the furnace and as-fired coal particle size, indicating that the maximum pressure in the furnace Pmax gradually increased with decreasing as-fired coal particle size. The maximum pressure was 703 Pa when the particle size was 40 mm, and it rose up to 4,184 Pa at 5 mm particle size.

Table 5 Maximum pressures of different particle sizes of as-fired coal.

D/mm	40	35	30	25	20	15	10	5
P_{max}/Pa	703	968	1200	1498	1816	2308	3178	4184

Figure 12 shows the relationship between the maximum pressure in the furnace and particle size. It is obvious that the maximum pressure in the furnace approximately increased exponentially from 703 Pa to

4,184 Pa when particle size decreased from 40 mm to 5 mm. The exponential fitting of the relationship between the maximum pressure in the furnace and particle size showed a correlation coefficient of 0.9970. The fitting equation is as follows:

$$P_{max} = 5236.89 \times e\text{-}D/15.8345 + 359.868 \quad (3)$$

3.6 Comparative analysis between simulation data and factory test data

Tables 6 and 7 provide the temperatures and pressures of various factory measuring points. Figure 13 show the data based fitting curves.

Table 6 Temperature statistics of various measuring points.

/mm	32.44	16.97	14.76	12.55	8.13
$T_{Z=1}$/K	842	738	710	682	640
$T_{Z=2.5}$/K	1003	937	929	910	879
T_{max}/K	1114	1023	1008	977	926

Table 7 Pressure statistics of various measuring points.

/mm	32.44	16.97	14.76	12.55	8.13
$P_{Z=2}$/Pa	893	2021	2274	2549	3168
$P_{Z=4.5}$/P	855	1829	2043	2276	2799
P_{max}/Pa	970	2225	2509	2820	3519

Figure13 provide the polynomial temperature curves at the maximum temperature in the furnace (T_{max}) and at the heights of z = 1 and z = 2.5, respectively, and the polynomial pressure curves at the maximum pressure (P_{max}) and at the heights of z = 2 m and z = 4.5 m, fitted according to the eight groups of temperature and pressure data measured at the corresponding positions in the furnace in the factory when particle size decreased from 40 mm to 5 mm. As shown in Figure 13(a), the simulation values basically matched with the experimental values. According to the computational data, the maximum temperature error was 6.25% when the average particle size and height were 8.13 and 1 m, respectively. As shown in Figure 13(b), the simulation values also basically matched with the experimental values. The maximum pressure error was 12.8% when the average particle size and height were 32.44 and 4.5 m, respectively according to the computational data.

4. Conclusions

The three-dimensional temperature and pressure field of SJ low temperature carbonization furnace was first simulated by CFD, separately. The temperature field distribution presented an increasing trend first and decreasing afterwards when the same particle size coal entered the SJ furnace. The trends of temperature field distribution were similar when different particle sizes of coal entered the SJ furnace. However, temperature declined with decreasing particle size. The pressure in the furnace cavity (except the furnace outlet) presented an approximately linear decline when the same particle size of coal entered the furnace. The pressure increased with decreasing particle size when different particle sizes coal entered the furnace. Moreover, the comparison between the simulation data and the industrial test data in the furnace revealed a temperature error lower than 6.25% and a pressure error lower than 12.8%, which conformed to the production conditions basically and provided an important theoretical basis for further studies on SJ carbonization furnace.

Declarations

This work was financially supported by the National Natural Science Foundation of China(No.21663034), the Science and Technology Plan of Shaanxi Province, China(No.2016KTZDGY08-04-01, No.2020TD-031, No.2020JQ-901), the Science and Technology Plan of Yulin Government, China(No.2016CXY-18, No.2018-2-44).

References

[1] LIN Yuan-kui, LIQing-song, LI Xue-feng, ZHANG Kang, YU Ying-min, SONG Yu-he, FU Yu, SUN Lan-yi. Pyrolysates distribution and kinetics of Shenmu long flame coal [J]. Energy Conversion and Management, 2014, 86: 428-434.

[2] XUE Feng-feng, LI Dong, GUO Yu-ting LIU Xu ZHANG Xiang-ping, ZHOU Qiu-cheng, MA Bao-qi. Technical Progress and the Prospect of Low-Rank Coal Pyrolysis in China [J]. Energy Technology, 2017, 5(11): 1897-1907.

[3] YANG Jian-li, Stansberry P G, Zondlo J W, Stiller A H. Characteristics and carbonization behaviors of coal extracts [J]. Fuel Processing Technology, 2002, 79(3): 207-215.

[4] LIANG Peng, ZHANG Ya-qing, JIANG Wan-min, WEI Ai-fang, LIU Tao, WU Jia-feng. Simulation Study of Shenmu Coal Pyrolysis by Gas Heat Carrier Based on a Moving Bed [J]. Energy Fuels, 2015, 29 (11): 7727-7733.

[5] HOU Ji-li, MA Yue, LI Shu-yuan, SHANG Wen-zhi. A comparative study on characteristics of sulfur and nitrogen transformation and gaseous emission for combustion of bituminous coaland char [J]. Carbon Resources Conversion, 2018, 1(1): 86-93.

[6] HOU Ji-li, MA Yue, LI Shu-yuan, SHI Jian, He Lu, LI Jia. Transformation of sulfur and nitrogen during Shenmu coal pyrolysis [J]. Fuel, 2018, 231, 134-144.

[7] YOU Quan, WU Shi-yong, WU You-qing, HUANG Sheng, GAO Jin-sheng, SHANG Jian-xuan, MIN Xiao-jian, ZHENGHua-an. Product distributions and characterizationsfor integrated mild-liquefaction and carbonization of low rank coals [J]. Fuel Processing Technology, 2017, 156, 54-61.

[8] SINGH R I, BRINK A, HUPA M. CFD modeling to study fluidized bed combustion and gasification [J]. Applied Thermal Engineering, 2013, 52(2): 585-614.

[9] SANKAR G, SANTHOSHKUMAR D, BALASUBRAMANIAN K R. Computational modeling of pulverized coal fired boilers – A review on the current position [J]. Fuel, 2019, 236, 643-665.

[10] YIN Chun-gen, YAN Jin-yue. Oxy-fuel combustion of pulverized fuels: Combustion fundamentals and modeling [J]. Applied Energy, 2016, 162, 742-762.

[11] GUO Zhan-chen, TANG Hui-qing. Numerical Simulation for a Process Analysis of a Coke Oven [J]. China Particuology, 2005, 3(6):373-378.

[12] SLEZAK A, KUHLMAN J M, SHADLE L J. CFD simulation of entrained-flow coal gasification:Coal particle density/size fraction effects [J]. Powder Technology, 2010, 203:98-108.

[13] LIU Jun, ZHANG Yong-fa, WANG Ying, CHEN Lei, XU Ying, ZHAO Hai-bin. Temperature distribution simulation and structural optimization of low-temperature combustion chamber in carbonization furnace [J]. Chemical Industry and Engineering Progress, 2013, 32(9): 2112-2119.

[14] ZHANG Qiu-li, HU Xiao-yan, ZHAO Xi-cheng, LAN Xin-zhe, SONG Yong-hui. Impact of the ratio of re-blow coal gas and air on temperature field in low temperature dry distillation furnace [J]. Coal Conversion, 2012, 35(2): 56-60. (in Chinese)

[15] SELMA B, BANNARI R, PROULX P. A full integration of a dispersion and interface closures in the standard k–ε model of turbulence [J]. Chemical Engineering Science, 2010, 65(20): 5417-5428.

[16] ZHANG Chun-jie, XU Guo-qiang, SUN Jin-ing, ZHAO Jin. Modified k–ε model for RP-3 kerosene in a horizontal circular tube at supercritical pressure [J]. Applied Thermal Engineering, 2016, 102, 1403-1411.

[17] LIU Dai-fei, DING Feng-qi, ZHANG Hong-liang, ZHANG Wen-bo. Numerical simulation of high temperature air combustion in aluminum hydroxide gas suspension calcinations [J]. Transactions of Nonferrous Metals Society of China, 2009, 19(1): 259-266.

[18] KE Cun-feng, ZHANG Yan-ying, GAO Ya-nan, LIU Shi-yu, PAN Yao-yu, ZHOU Nan, WANG Yun-pu, FAN Liang-liang, PENG Peng, LI Bing-xi, RUAN Ro-ger. Syngas production from microwave-assisted air gasification of biomass: Part 1 model development [J]. Renewable Energy, 2019, 140, 772-778.

[19]SADHUKHAN A K, GUPTA P, SAHA R K. Modeling of Pyrolysis of Large Wood Particles [J]. Bioresource Technology, 2009, 100(12): 3134-3139.

[20] LU Xi-jia, WANG Ting. Investigation of radiation models in entrained-flow coal gasification simulation [J]. International Journal of Heat and Mass Transfer, 2013, 67, 377-392.

[21] SHANG Da, LI Bao-kuan, LIU Zhong-qiu. Large eddy simulation of transient turbulent flow and mixing process in an SCR denitration system [J]. Chemical Engineering Research and Design, 2019, 141, 279-289.

[22] GAO Xi, ZHU Ya-ping, LUO Zheng-hong. CFD modeling of gas flow in porous medium and catalytic coupling reaction from carbon monoxide to diethyl oxalate in fixed-bed reactors [J]. Chemical Engineering Science, 2011, 66(23): 6028-6038.

[23] CHANDRAN K B,VONESH M J, ROY A, GREENFIELD S, KANE B, Greene R,MCPHERSON D D. Computation of vascular flow dynamics from intravascular ultrasound images [J]. Medical Engineering & Physics, 1996, 18(4): 295-304.

[24] ALVARADO R C E, KLAPP J, SIGALOTTI L D G, DOMINGUEZ J M. Nonreflecting outlet boundary conditions for incompressible flows using SPH [J]. Computers & Fluids, 2017, 159, 177-188.

[25] DIXON A G, NIJEMEISLAND M, STITT E H. Packed Tubular Reactor Modeling and Catalyst Design using Computational Fluid Dynamics [J]. Advances in Chemical Engineering, 2006, 31, 307-389.

[26] WANG Hao-li, WANG Yuan. Influence of three-dimensional wall roughness on the laminar flow in microtube [J]. International Journal of Heat and Fluid Flow, 2007, 28(2): 220-228.

[27] IBRAHIMOGLU B, CUCEN A, YILMAZOGLU M Z. Numerical modeling of a downdraft plasma gasification reactor [J]. International Journal of Hydrogen Energy, 2017, 42(4): 2583-2591.

[28] ZHUO Yu-ting, SHEN Yan-song. Modelling of the pyrolysis of low-rank-coal briquettes in an industrial-scale gas heat carrier pyrolyzer [J]. Powder Technology, 2020, 361, 52-61.

[29] ERGUN S. Fluid flow through packed columns. Chemical Engineering Progress, 1952, 48(2):89-94.

[30]FRUHSTORFER J, ANEZIRIS C G. Influence of particle size distributions on the density and density gradients in uniaxial compacts [J]. Ceramics International, 2017, 43(16): 13175-13184.

[31] YUAN Chen-heng, JING Yuan, LIU Chun-zhi. He Yi-tuan. Effect of variable stroke on fuel combustion and heat release of a free piston linear hydrogen engine [J]. International Journal of Hydrogen Energy, 2019, 44(36): 20416-20425.

[32] HUANG Xue-chi, LI Bao-kuan, LIU Zhong-qiu. A coupled mathematical model of oxygen transfer in electroslag remelting process [J]. International Journal of Heat and Mass Transfer, 2018, 120,458-470.

[33] CHEN Lin, WEI Hao-qiao, CHEN Ce-yuan. Numerical investigations on the effects of turbulence intensity on knocking combustion in a downsized gasoline engine [J]. Energy, 2019, 166, 318-325.

[34] ZHANG Hu, LI Yue-ming, TAO Wen-quan. Effect of radiative heat transfer on determining thermal conductivity of semi-transparent materials using transient plane source method [J]. Applied Thermal Engineering, 2017, 114, 337-345.

[35] LI Yang, YANG Zhao-zhong, LI Xiao-gang. Molecular Simulation Study on the Effect of Coal Rank and Moisture on CO_2/CH_4 Competitive Adsorption [J]. Energy & Fuels, 2019, 33(9): 9087-9098.

[36] SCHOBERT H. Production of Acetylene and Acetylene-based Chemicals from Coal [J]. Chemical Reviews. 2014, 114(3): 1743-1760.

[37]POTTER O. Crossflow gas-particle heat and mass transfer and chemical reaction [J]. Chemical Engineering Research and Design, 2013, 91(2): 244-253.

[38] KATALAMBULA H, GUPTA R. Low-grade coals: A review of some prospective upgrading techmologies [J]. Energy & Fuels, 2009, 23(7): 3392-3405.

[39] GRANDA M, BLANCO C, ALVAREZ P, PATRICK J W, MENENDEZ R. Chemicals from Coal Coking [J]. Chemical Reviews, 2014, 114(3): 1608-1636.

[40] MORGAN T J, KANDIYOTI R. Pyrolysis of Coals and Biomass: Analysis of Thermal Breakdown and Its Products [J]. Chemical Reviews, 2014, 114(3): 1547-1607.

[41] JENSEN B, JACOBSEN N G, Christensen E D. Investigations on the porous media equations and resistance coefficients for coastal structures [J]. Coastal Engineering, 2014, 84, 56-72.

[42] SUN Zhi-wei, WEN Jian-hui, LUO Xiao, DU Wen, LIANG Zhi-wu, FU Kai-yun. An improved CFD model of gas flow and particle interception in a fiber material [J]. Chinese Journal of Chemical Engineering, 2017, 25(3): 264-273.

Figures

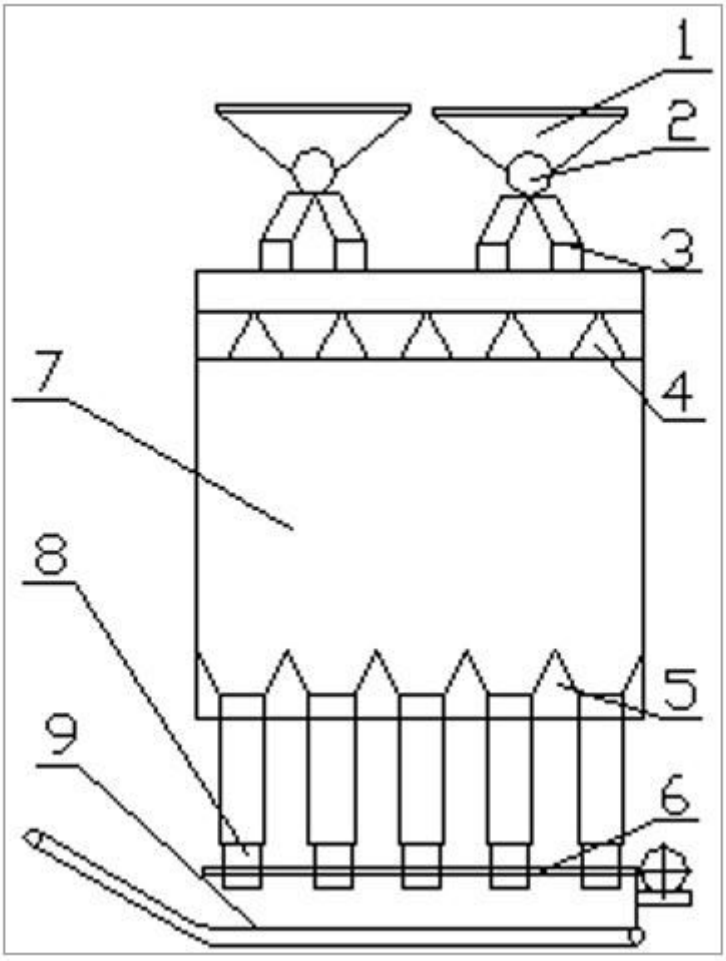

Figure 1

Structural sketch of low temperature carbonization furnace (1: coal hopper, 2: coal discharge valve, 3: auxiliary coal box, 4: gas collecting mantle, 5: grid wall, 6: coke pusher, 7: furnace cavity, 8: coke guide, 9: scraper).

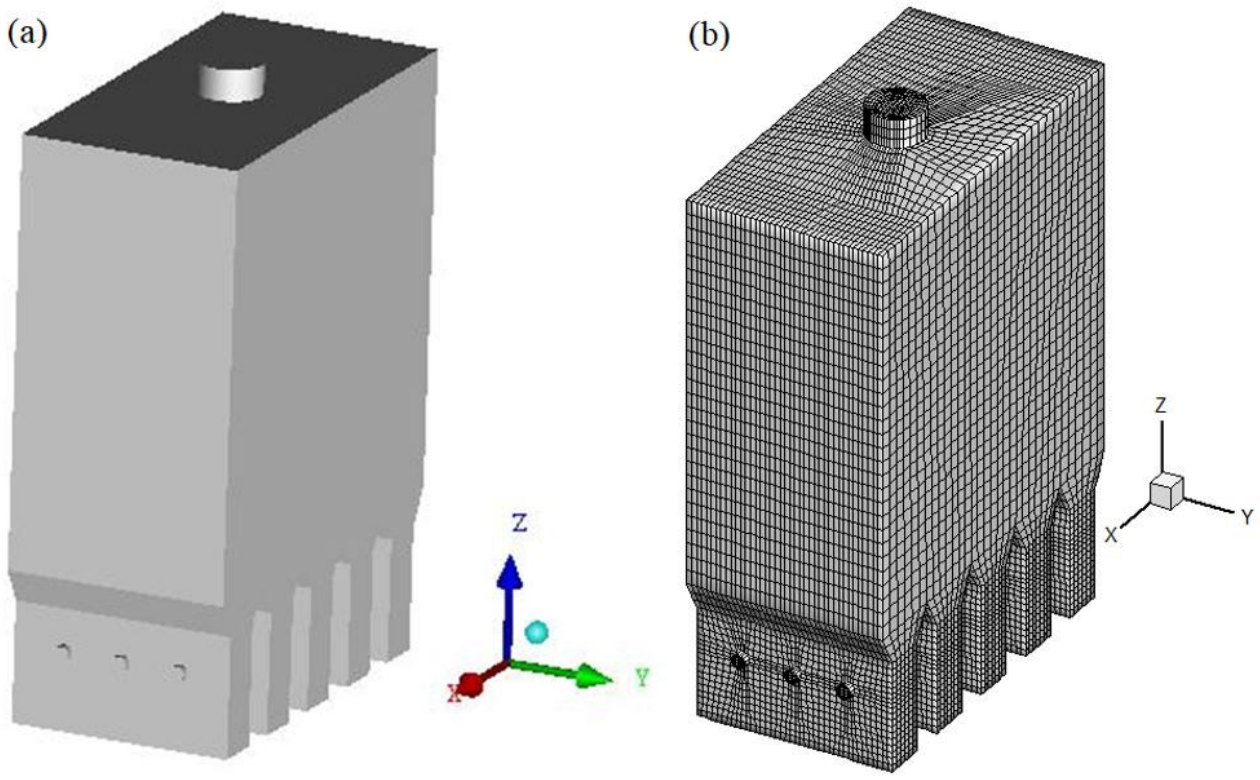

Figure 2

3D model diagram and Meshing diagram of SJ furnace.

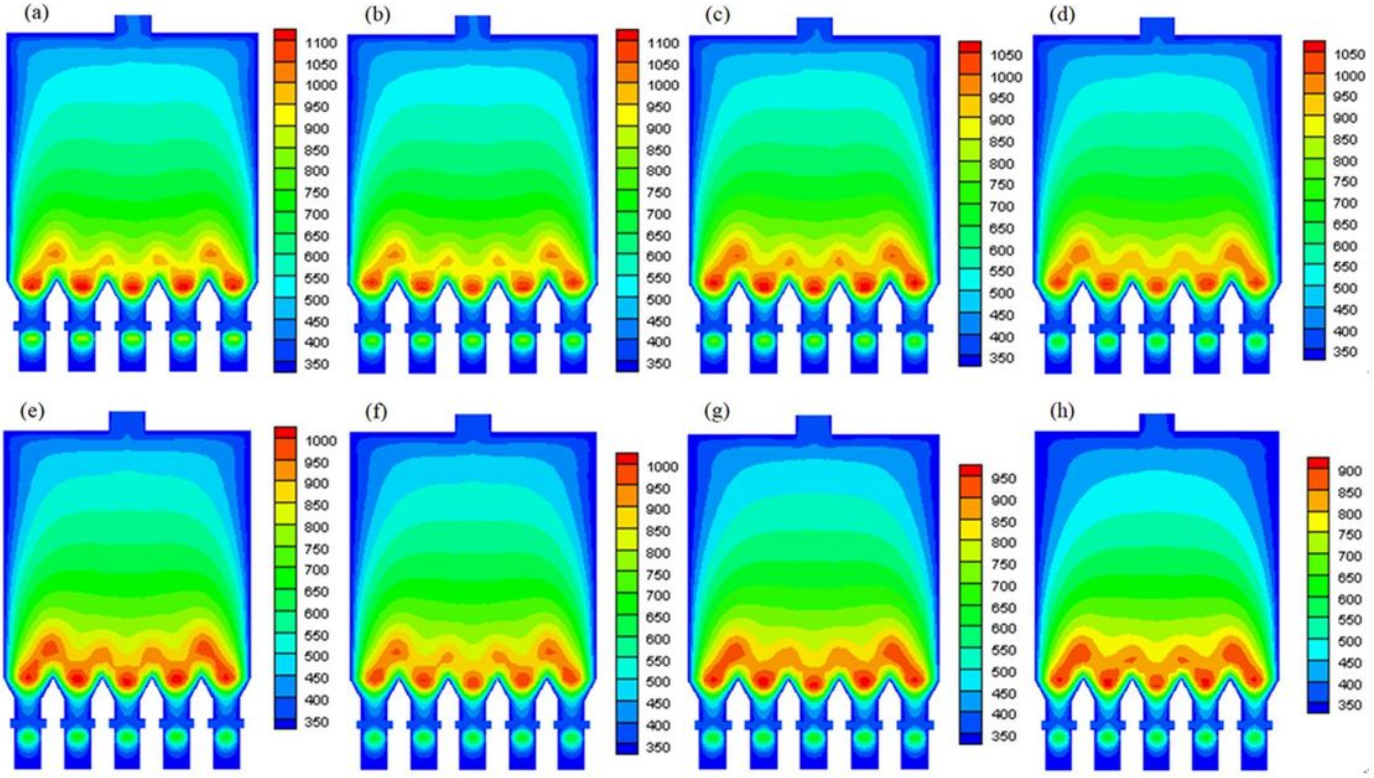

Figure 3

Temperature distribution (K) ofy-direction center section for different particle sizes of coal. (a: D=40mm; b: D=35mm; c: D=30mm; d: D=25mm; e: D=20mm; f: D=15mm; g: D=10mm; h: D=5mm).

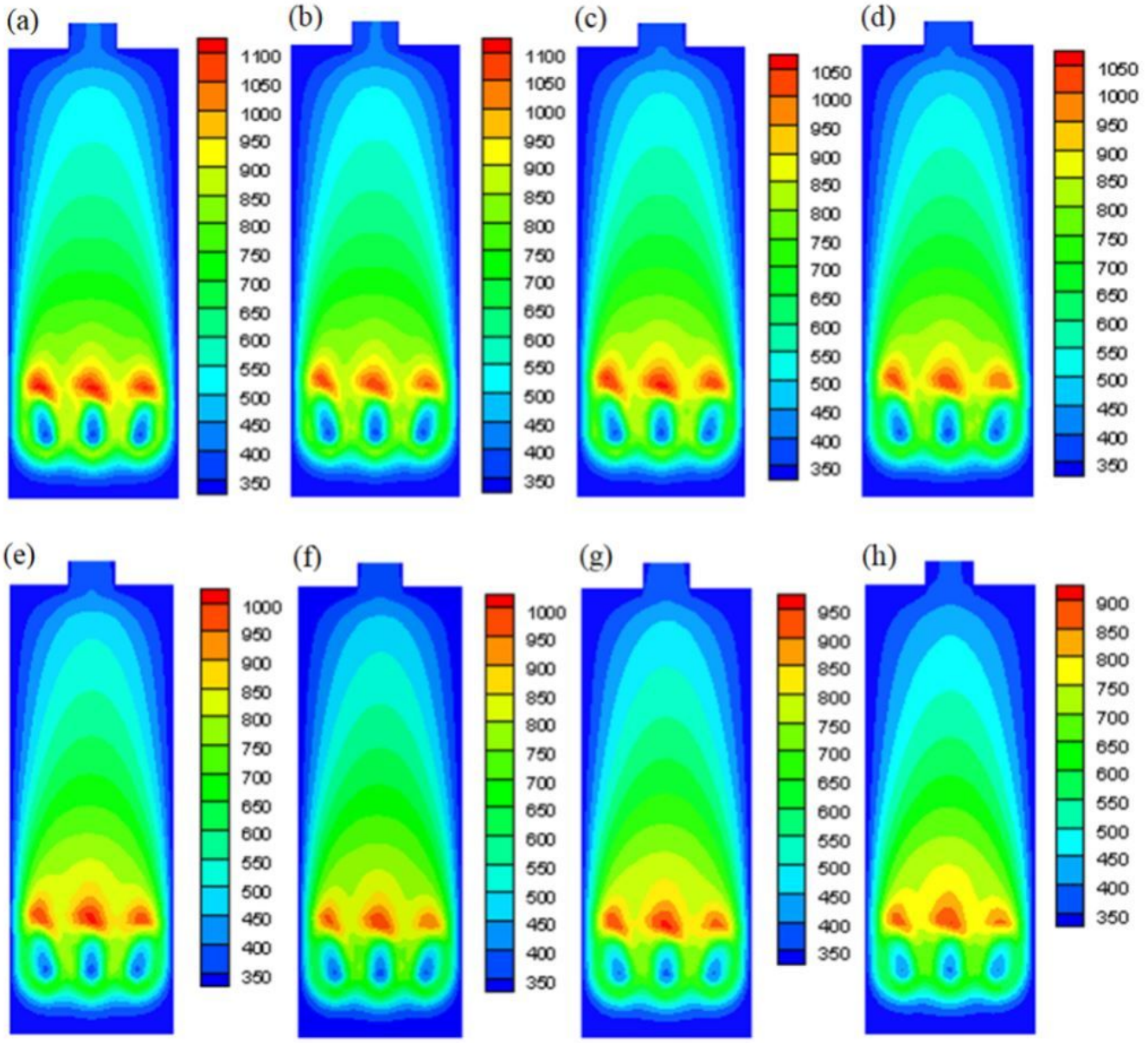

Figure 4

Temperature distribution (K) ofx-direction center section for different particle sizes of coal. (a: D=40mm; b: D=35mm; c: D=30mm; d: D=25mm; e: D=20mm; f: D=15mm; g: D=10mm; h: D=5mm).

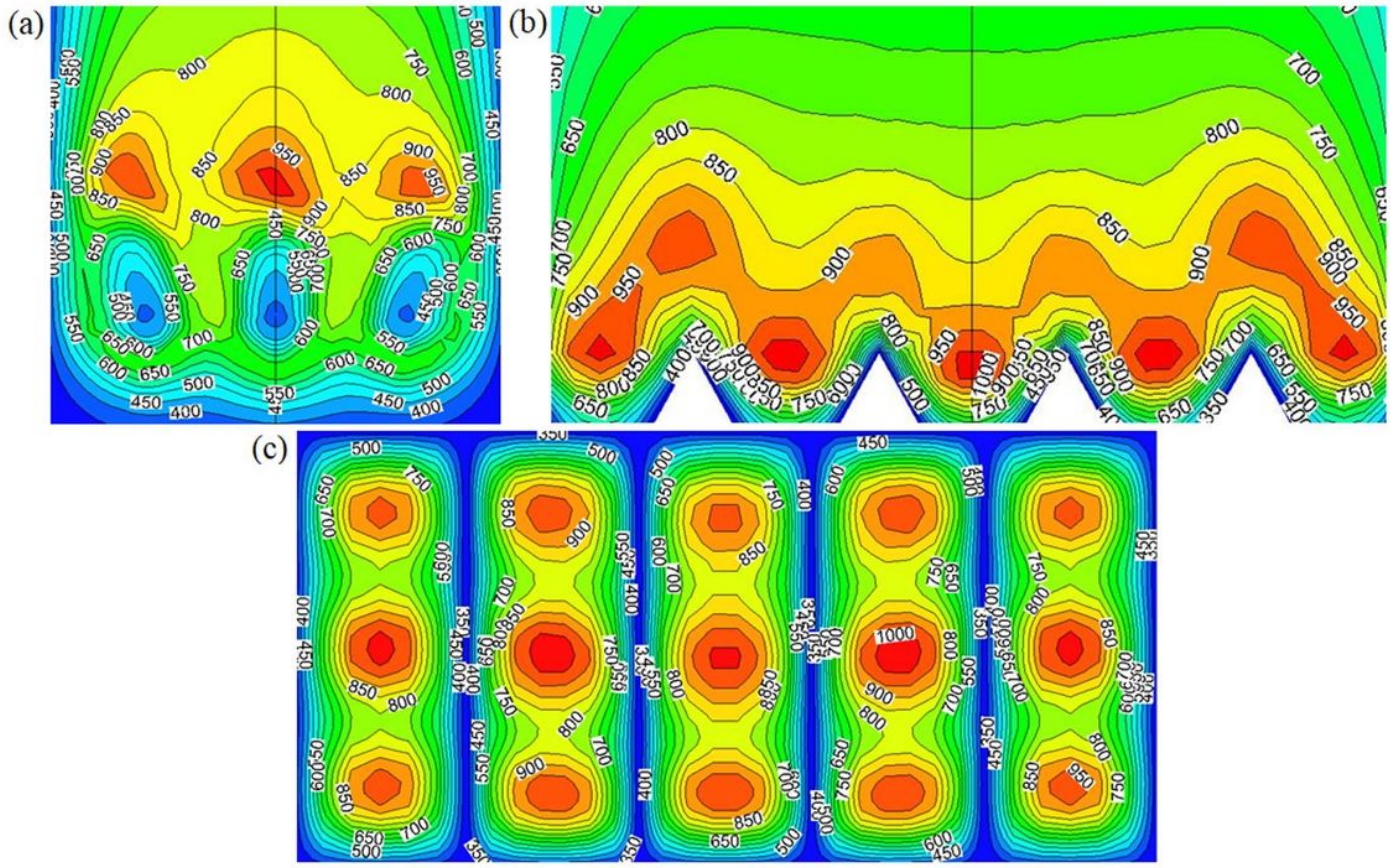

Figure 5

Partial enlarged drawing (K) of the high-temperature zone section (D = 20 mm). (a: x = 2.75 m; b: y = 1.4 m; c: z = 0 m)

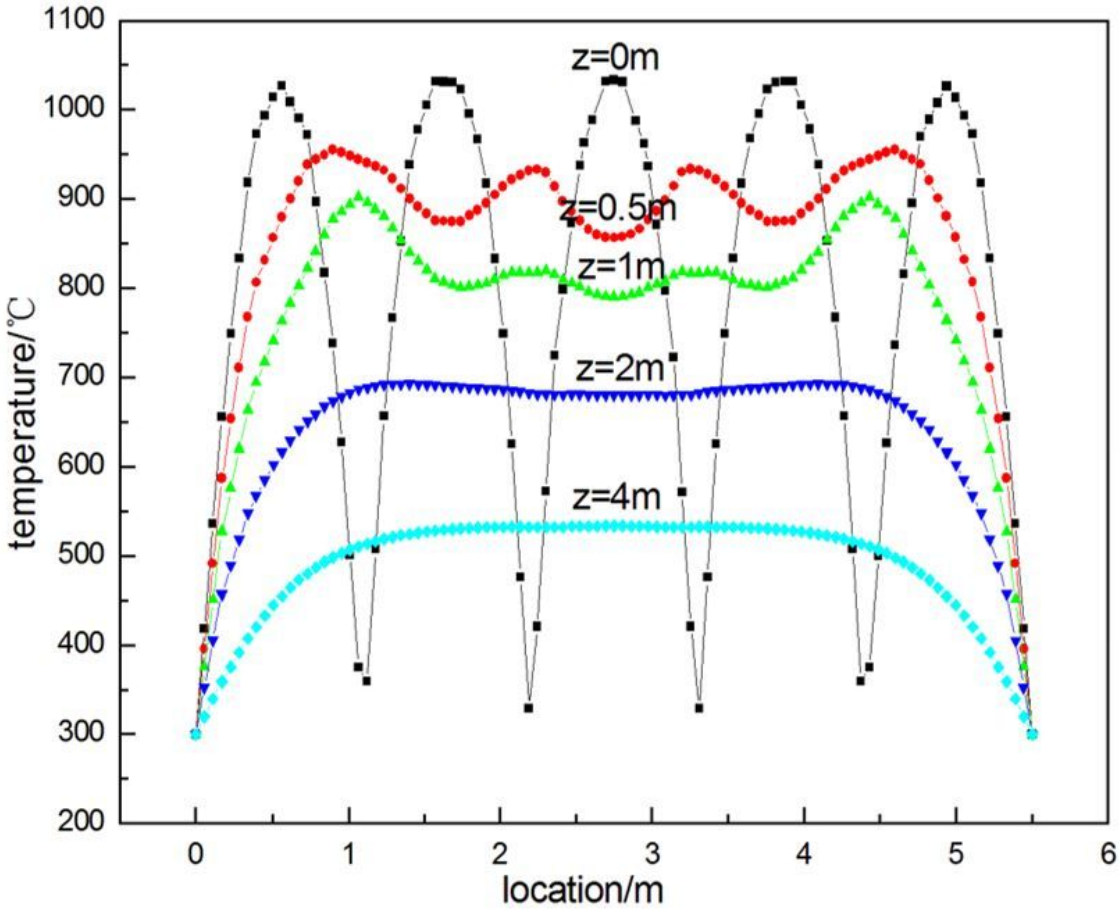

Figure 6

Temperature field distribution of longitudinal center section at different coal seam heights.

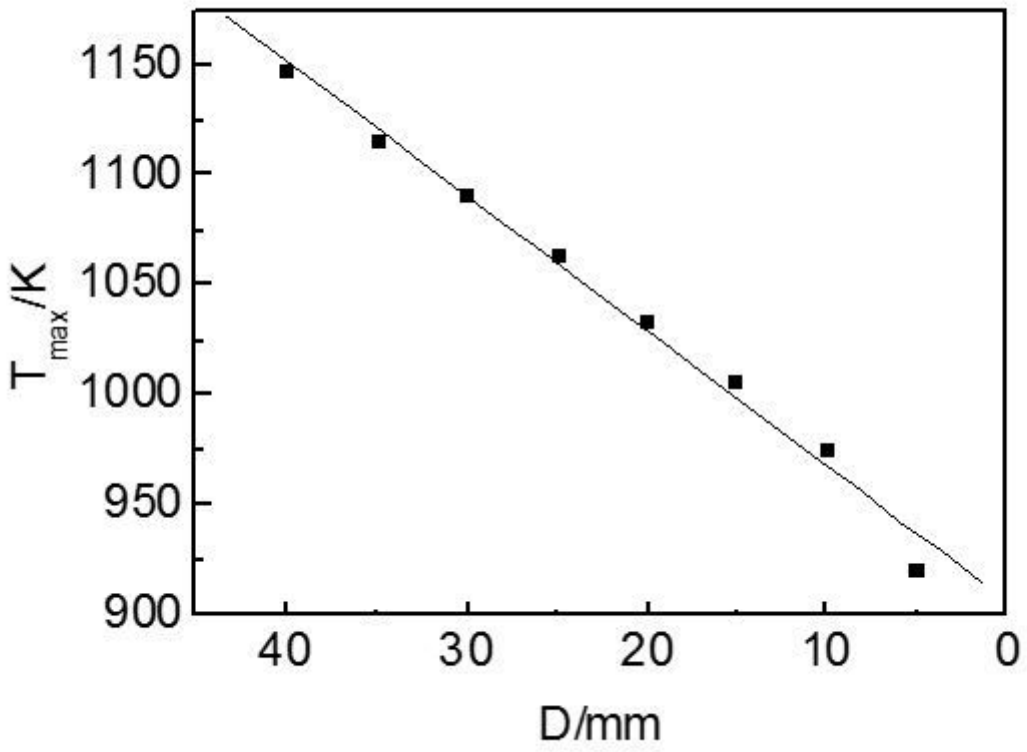

Figure 7

Relationship betweenmaximum temperature in furnace and particle size.

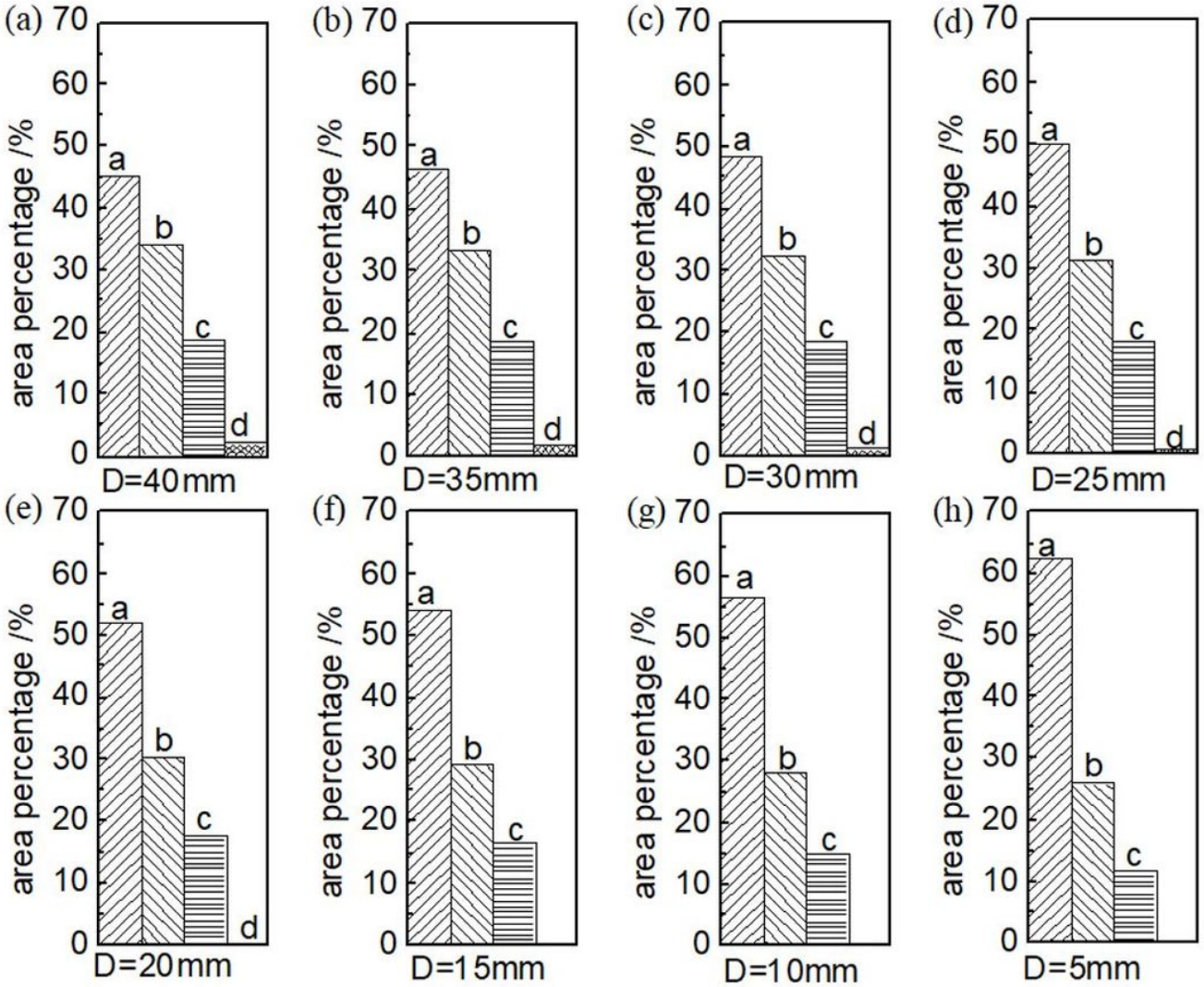

Figure 8

Volume percentage distributionof temperature ranges in the furnace cavity forcoal with different particle sizes (a: lower than 573 K; b: 573~773 K; c: 773~1,023 K; d: higher than 1,023 K).

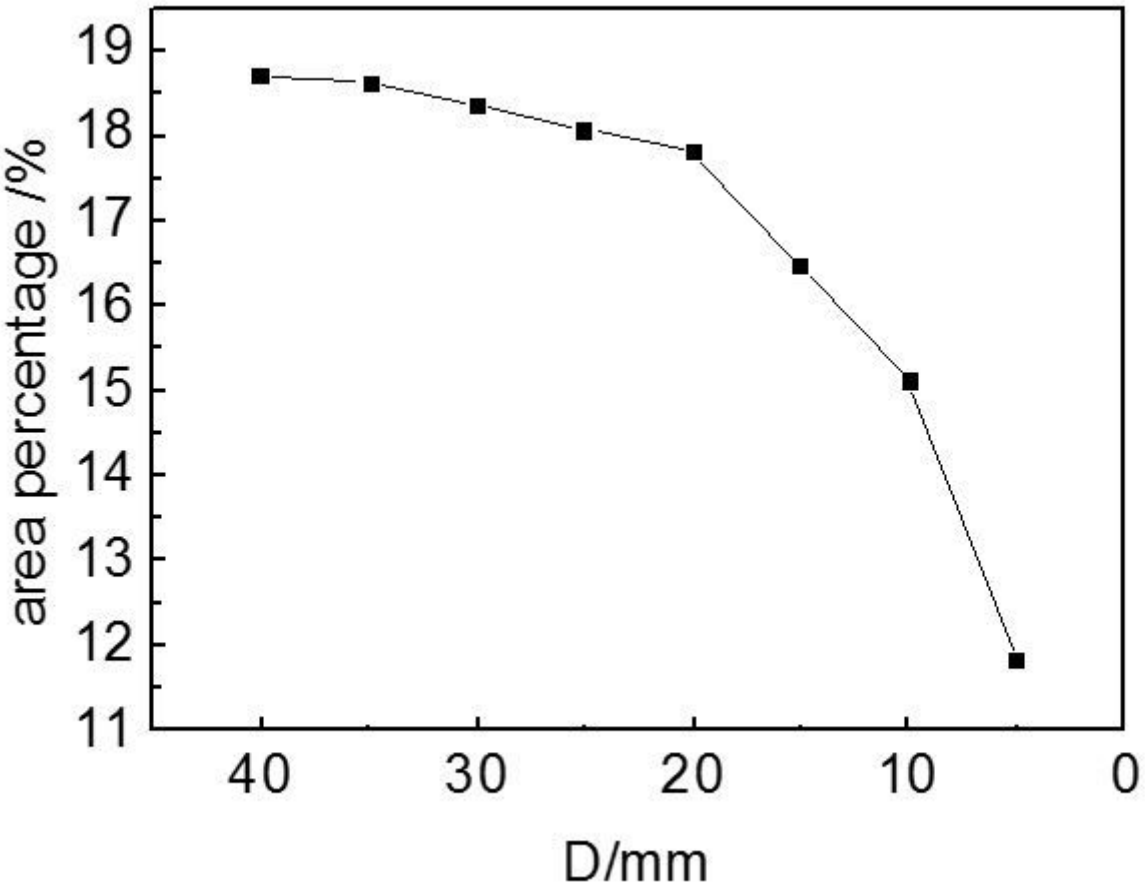

Figure 9

Volume percentages of thecarbonization zone for different particle sizes of coal.

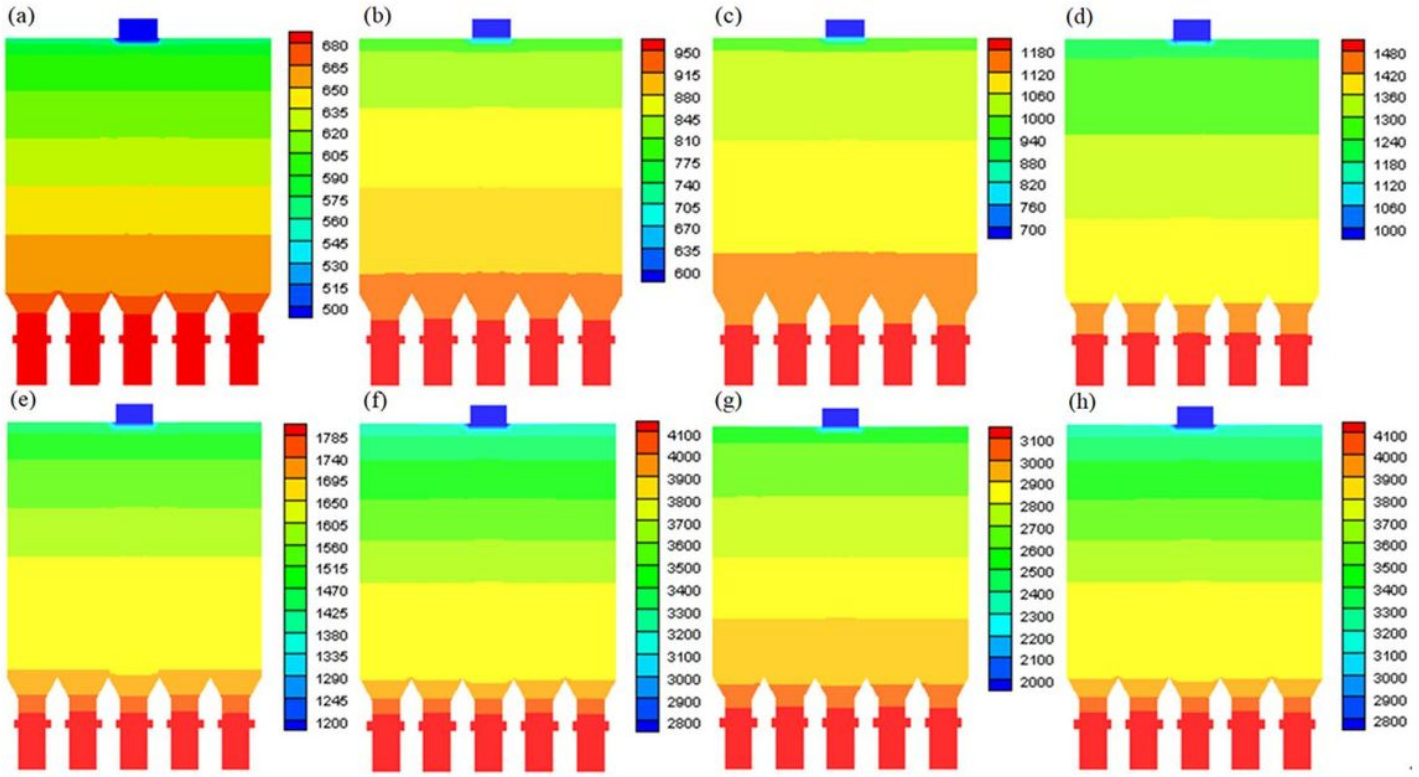

Figure 10

Pressure distribution (Pa) of y-direction center section for coal with different particle sizes.

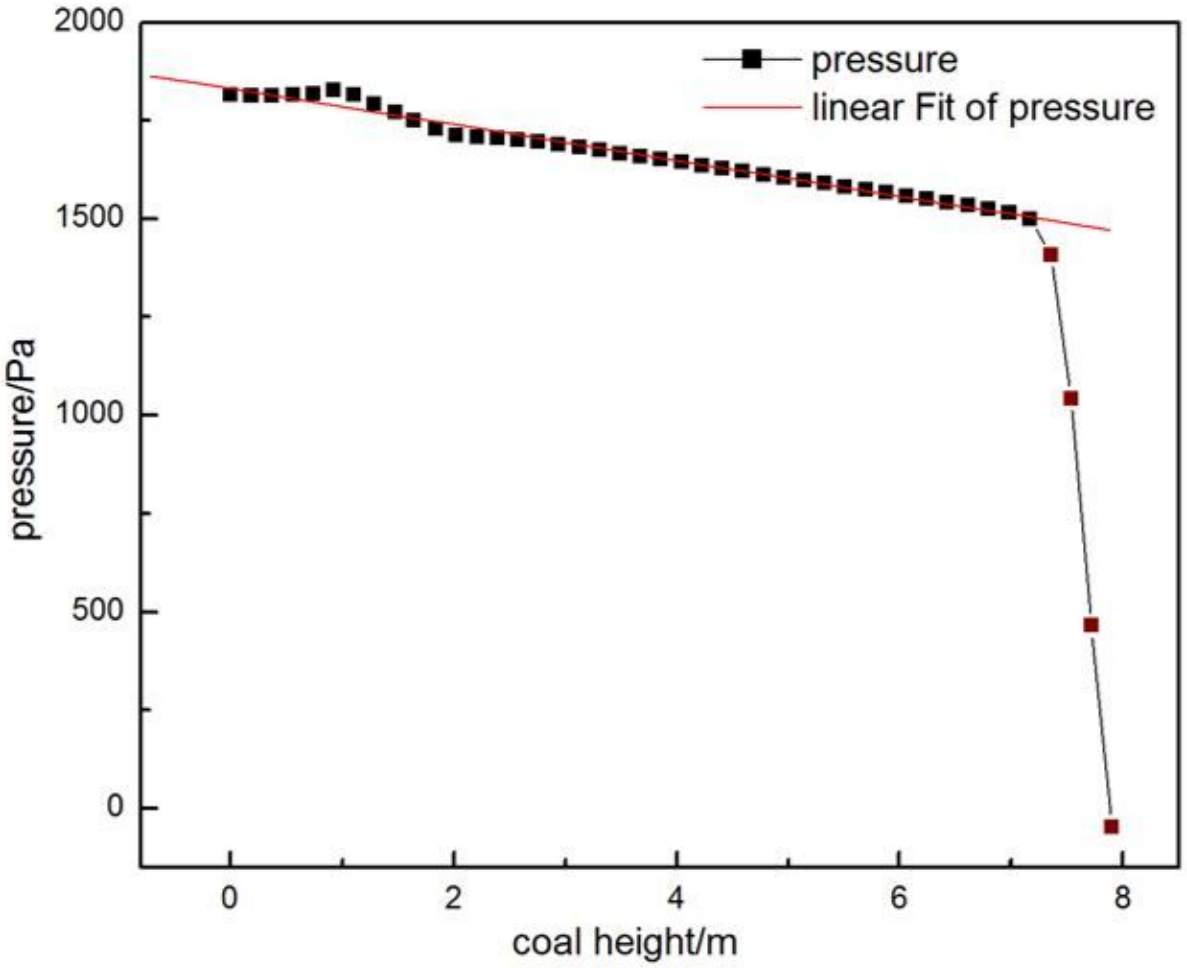

Figure 11

Pressure distributionin coal seam height direction in furnace (Pa).

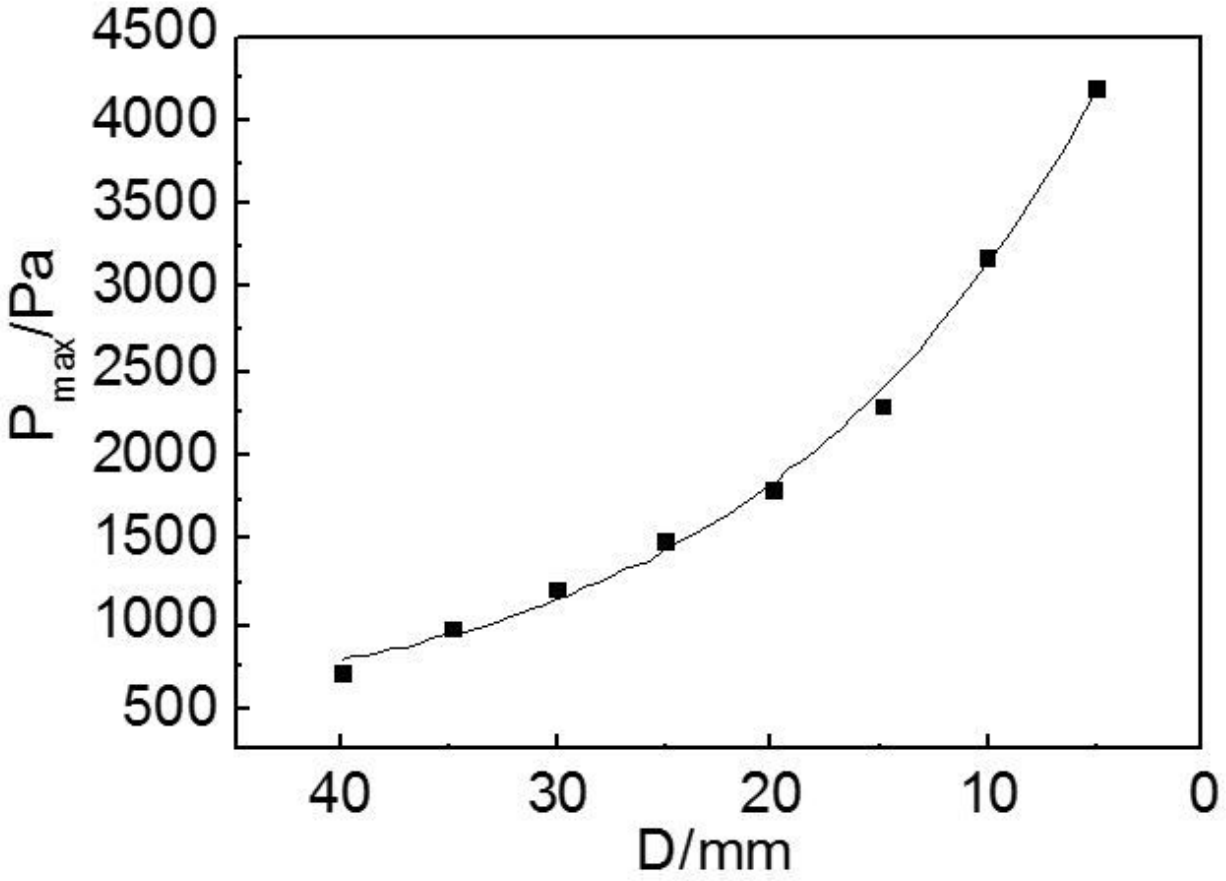

Figure 12

Relationship betweenmaximum pressure in furnace and particle size.

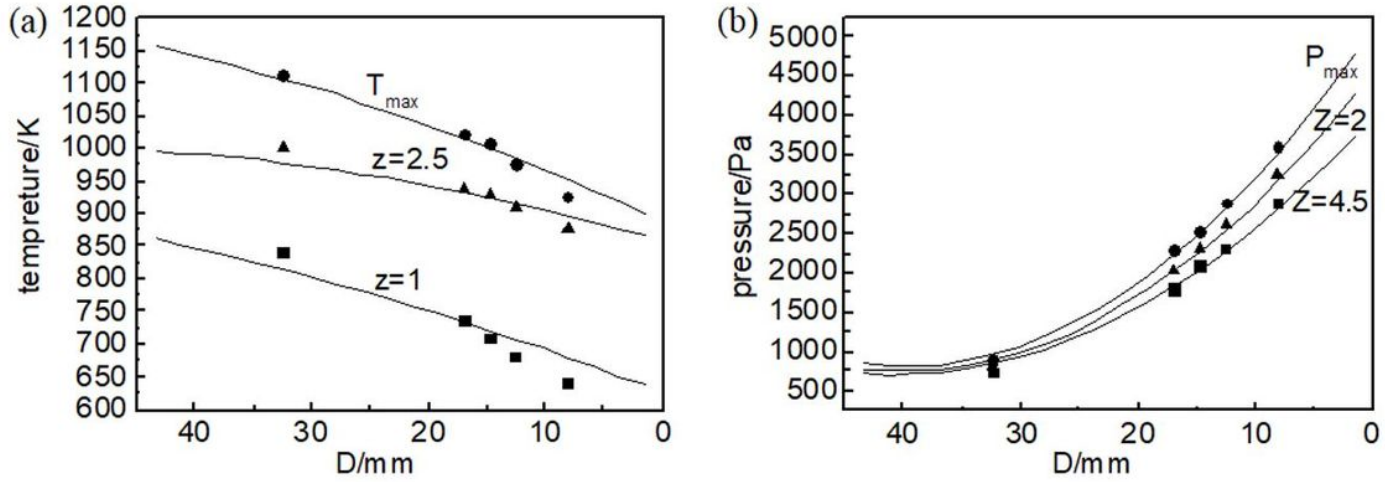

Figure 13

Change map of temperaturesimulation and pressure simulation at factory measuring points. (a: Temperaturesimulation; b: Pressure simulation)